JOINT INSTITUTE FOR NUCLEAR RESEARCH
Veksler and Baldin laboratory of High Energy Physics

FINAL REPORT ON THE INTEREST PROGRAMME

Soft photon study in hadron and nuclear interactions

Supervisor:
Prof. Elena Kokoulina

Student:
An Binh Le, Vietnam
University of Science

Participation period:
June 13 – July 29, Wave 7

Dubna, 2022

1. Introduction

There has been no thorough understanding of the process of soft photon production for almost 30 years. Soft photons (SPh) are the end result of high-energy interactions. They are not secondary particle decay products, and their energy is less than 50 MeV.

Data from experiments show that they have an excess of yield in hadron and nuclear interactions. Existing theoretical calculations based on quantum electrodynamics are incapable of predicting and explaining this excess. The construction of the future accelerator complex NICA allows for further in-depth research of this phenomena in various interactions.

SPh's nature has been a mystery till now. They appear to emerge in the realm of non perturbative quantum chromodynamics, and scientists construct phenomenological models. The most effective model is based on the cold quark-gluon plasma (QGP) creation theory. This model predicts the development of a quark-gluon system composed of a few quarks, antiquarks, and gluons (about 40 partons). Because they lack the energy to generate hadrons, these partons collide and reradiate soft photons, with the primary responses being Compton scattering and pair annihilation.

2. Project goal

- Getting accustomed to Geant4 packet and CERN Root open-source data analysis framework.
- Data taking and data processing for different simulations.
- Study of the operation of electromagnetic calorimeters of heterogeneous ‘spaghetti’ and ‘shashlik’ types.

3. Interaction of radiation with matter

Particles and radiation can be detected only through their interactions with matter. There are specific interactions for charged particles which are different from those of neutral particles, e.g. of photons. One can say that every interaction process can be used as a basis for a detector concept. The variety of these processes is quite rich and, as a consequence, a large number of detection devices for particles and radiation exist. In addition, for one and the same particle, different interaction processes at different energies may be relevant.

When radiation passes through matter there can be the following interactions:

- Interactions with the atom for radiation with a wavelength of the order of the size of the atom (a few angstroms). In the majority of cases the interaction takes place with atomic electrons, for example; the photoelectric effect or the Compton Effect. We can also have the diffraction of electromagnetic waves or beams of electrons by a set of atoms or crystals.
- Interactions with the atomic nucleus for radiation of wave length of the order of the size of the nucleus, this is the case of nuclear reactions.
- Interactions with nucleons (constituents of the atomic nucleus; neutrons and protons) for high energy radiation, this is the case with particle bombardment in high energy particle accelerators.

In a general way, each interaction has a certain probability of occurring. This probability depends on the nature and energy of the radiation.

3.1. Radiation length $\left(X_0\right)$

The average energy loss by Bremsstrahlung (photon emission in the electromagnetic field of a nucleus) increases almost linearly as a function of incident energy. This is described by introducing the radiation length defined X_0

$$-\frac{dE}{E}=\frac{dx}{X_0} \tag{1}$$

It can be calculated for a material composed of only one element

$$X_0=\frac{716.4\,A\left[g/mol\right]}{Z\left(Z+1\right)\ln\left(287/\sqrt{Z}\right)}\ g/cm^2 \tag{2}$$

The radiation length for a mixture of elements or a compound can be approximated by

$$X_0=\frac{1}{\sum_{i=1}^{N} f_i/X_0^i} \tag{3}$$

where f_i are the mass fractions of the components with the radiation length X_0^i.

The mass fraction can be calculated using the following formula

$$f_i=\frac{A_i v_i}{\sum_{i=1}^{N} A_k v_k} \tag{4}$$

where A_i and A_k are the atomic masses in g/mole have v_i and v_k valences of atom in molecule.

3.2. Critical energy (E_c)

Energy losses due to Bremsstrahlung are proportional to the energy while ionisation energy losses beyond the minimum of ionisation are proportional to the logarithm of the energy. The energy, where these two interaction processes for electrons lead to equal energy losses, is called the critical energy E_c

$$E_c = \frac{610\,\text{MeV}}{Z + 1.24} \tag{5}$$

For compound materials with N elements

$$E_c = \frac{550\,\text{MeV}}{Z_{\text{eff}}} \tag{6}$$

where Z_{eff} is an effective atomic number for a material that is a mixture of elements

$$Z_{\text{eff}} = \frac{\sum_{i=1}^{N} Z_i f_i}{\sum_{i=1}^{N} f_i} \tag{7}$$

3.3. Molière radius (R_M)

The Molière radius is defined by the ratio of radiation length and critical energy as

$$R_M = \frac{21\,\text{MeV}}{E_c} X_0 \ \text{g/cm}^2 \tag{8}$$

4. Calorimetry

The assumption behind calorimetric techniques is that the particle energy will be completely absorbed by a mass of material before the deposited energy will be measured. High-energy photons, electrons, and hadrons can interact with matter to produce secondary particles, which can result in the formation of a shower. The particle energy is then considerably more effectively deposited in the substance. Thus, the detection of electromagnetic and hadronic showers is the most common usage of calorimeters in high

energy physics. These detectors are referred to as electromagnetic and hadron calorimeters as a result.

4.1. Electromagnetic calorimeters

The dominating interaction processes for spectroscopy in the MeV energy range are the photoelectric and Compton effect for photons and ionisation and excitation for charged particles. At high energies (higher than 100 MeV) electrons lose their energy almost exclusively by Bremsstrahlung while photons lose their energy by electron–positron pair production.

After one radiation length the photon produces an e^+e^- pair; electrons and positrons emit after another radiation length one Bremsstrahlung photon each, which again are transformed into electron–positron pairs. Let us assume that the energy is symmetrically shared between the particles at each step of the multiplication.

This very simple model already correctly describes the most important qualitative characteristics of electromagnetic cascades.

- To absorb most of the energy of the incident photon the total calorimeter thickness should be more than $10-15\ X_0$.
- The position of the shower maximum increases slowly with energy. Hence, the thickness of the calorimeter should increase as the logarithm of the energy but not proportionally as for muons.
- The energy leakage is caused mostly by soft photons escaping the calorimeter at the sides (lateral leakage) or at the back (rear leakage).

In reality the shower development is much more complicated. An accurate description of the shower development is a difficult task. Earlier, large efforts were undertaken to develop an analytical approach. At present, due to the increase of the computer capacity, an accurate description is obtained from Monte Carlo simulations.

4.1.1. Homogeneous calorimeters

Homogeneous calorimeters are constructed from a material combining the properties of an absorber and a detector. It means that practically the total volume of the calorimeter is sensitive to the deposited energy. These calorimeters are based on the measurement of the scintillation light (scintillation crystals, liquid noble gases), ionisation (liquid noble gases) and the Cherenkov light (lead glass or heavy transparent crystals). The main parameters of electromagnetic calorimeters are the energy and position resolution for photons and electrons. The energy resolution σ_E/E is determined both by physical factors

like the fluctuation of the energy leakage or photoelectron statistics and technical ones like non-uniformity of crystals.

For all calorimeter types the common contribution to the energy resolution originates from fluctuations of the energy leakage and from fluctuations of the first interaction point. The energy resolution can be expressed as

$$\sigma_{int}^2 = \sigma_l^2 + \sigma_r^2 + \sigma_l^2 + \sigma_b^2 \quad (9)$$

where σ_l is determined by the fluctuations of the point of the first interaction, σ_r is the rear leakage, σ_l the lateral leakage and σ_b the leakage due to albedo fluctuations.

4.1.2. Heterogeneous calorimeters

The proposed spaghetti calorimeter consists of a passive absorber and scintillator rods laid out throughout the volume of the calorimeter, in the direction of the particle shower. In order to collect the emitted light, the scintillator rods are connected to a photomultiplier at the end. Proposed calorimeter has 11x11 rods equally spaced out, which makes the scintillator crystal about 24% of the calorimeter.

Proposed shashlik calorimeters consist of alternating layers of the passive absorber and active detector material. To collect the light emitted in the scintillator layers, wave-length shifter fibers are used throughout the calorimeter. The calorimeter model consists of 28 scintillator plates with dimensions 100×100×3 mm^3 and 27 plates of W/Cu absorber (100×100×2 mm^3).

5. Geant4 simulation

In this survey, inorganic materials NaI, BGO and GaGG are respectively used to simulate two types of heterogeneous calorimeters, SpaCal and Shashlik. With the combination of the absorber to absorb as much of the particle energy as possible and therefore shorten the calorimeter thickness, the absorber material would ideally have to be very dense and with a small radiation length. However, using only Tungsten is very expensive. For the purpose of this simulation, a 50% Cu + 50% W composite is proposed, as a balance between the cost and density/radiation length.

Table 1. Properties of W and Cu

Element	Z	A (g/mol)	ρ (g/cm^3)	X_0 (cm)
W	74	183.84	19.30	0.35
Cu	29	63.55	9.96	1.44

The radiation length for the WCu composite is given by

$$X_0^{WCu} = 0.8 \text{ cm}$$

and the density

$$\rho_{WCu} = 11.85 \text{ g/cm}^3$$

5.1. Spaghetti (SpaCal) GaGG calorimeter

Gadolinium-gallium garnet, $Gd_3Al_2Ga_3O_{12}$, is a newly developed inorganic scintillator. It is one of the brightest available scintillators with an emission peak at 520 nm. GaGG has good stopping power with the density 6.67 g/cm^3, is physically rugged and and well suited to a broad range of applications. Fibers made of GaGG were placed in WCu crystal in 11x11 grid. Dimensions of each fiber were 3x3x100 mm.

Table 2. Component properties of the GaGG scintillator.

Element	Z	A (g/mol)	v	ρ (g/cm3)	f	X_0 (cm)
Ga	31	69.72	3	5.91	0.22	2.16
Gd	64	157.25	3	8.64	0.50	0.87
Al	13	26.98	2	2.70	0.05	8.99
O	8	15.99	12	0.00143	0.21	24098.90

The radiation length for the Wcu composite is given by:

$$X_0^{GaGG} = 1.44 \text{ cm}$$

and the critical energy:

$$E_c^{GaGG} = 13.1 \text{ MeV}$$

For the Molière radius:

$$R_M^{GaGG} = 2.32 \text{ cm}$$

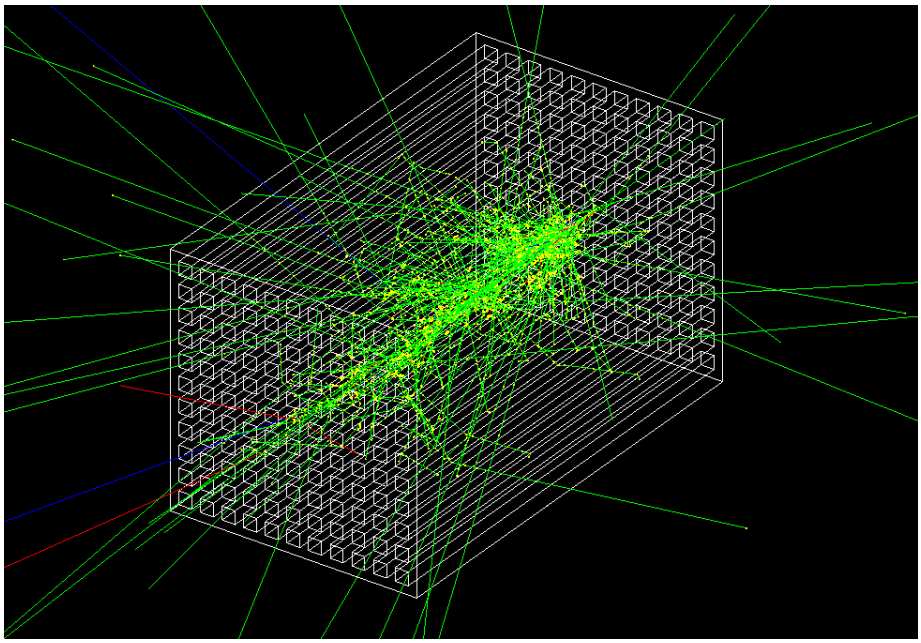

Figure 1. Simulation of electromagnetic shower in GaGG 'spaghetti' calorimeter (initial 50 MeV photons).

Energy resolution of fitted gaussian for E = 50 MeV is $\left(\frac{\sigma_E}{E}\right)_{GaGG} = 10.46\%$

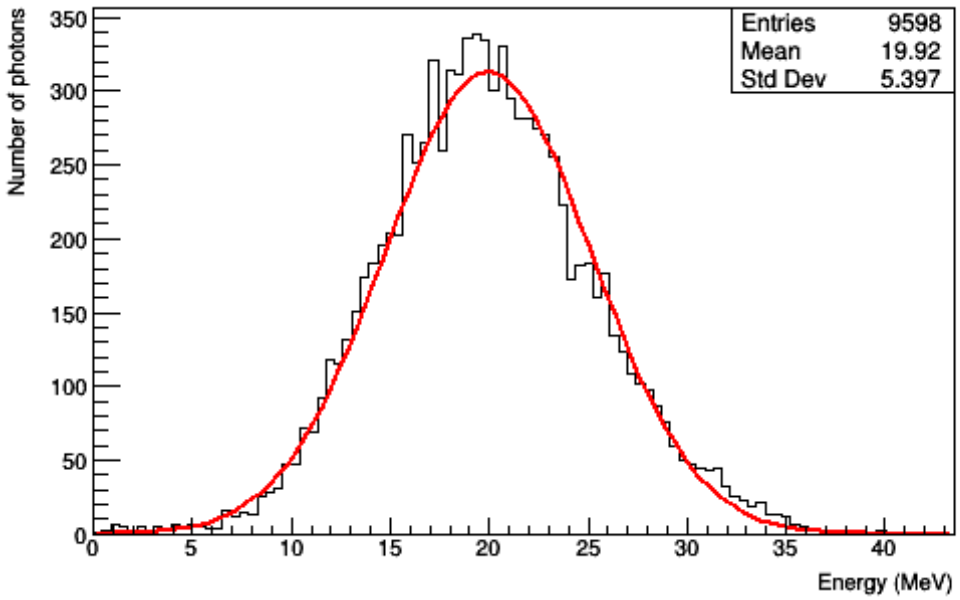

Figure 2. Energy deposition in fiber of GaGG calorimeter for 50 MeV photons.

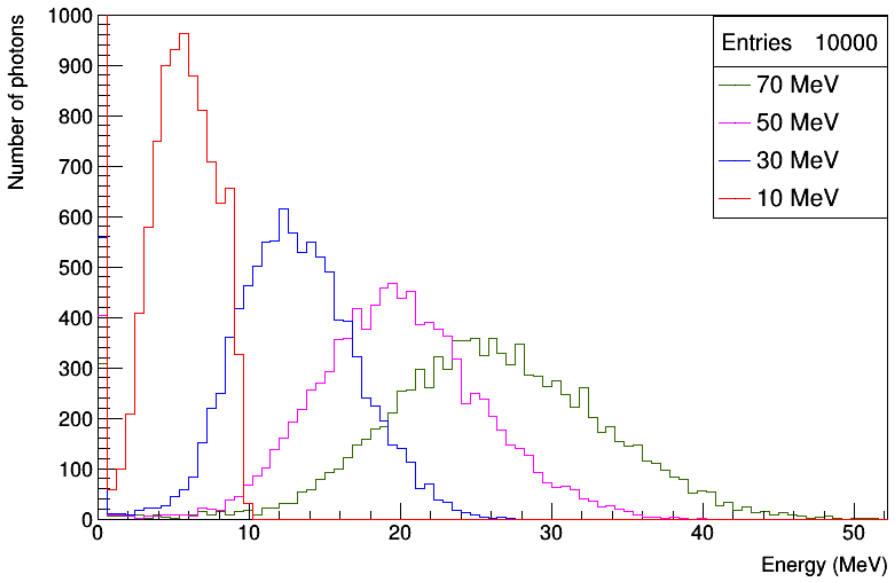

Figure 3. Various energy depositions in fiber of GaGG scintillator.

5.2. Spaghetti (SpaCal) NaI calorimeter

Sodium iodide (NaI) is a low-density, low-Z scintillator that is moderately sensitive to high-energy beta radiation and sensitive to low- and intermediate energy gamma radiation. Due to its excellent radiopurity, sodium iodide is used in several gamma-ray spectrometry techniques and is appealing for dark matter research applications. Because it may be produced in a variety of shapes and sizes, sodium iodide is less expensive to create. Additionally, it has a strong light output at short wavelengths, making it compatible with many other photomultiplier tubes. It offers high quality and efficiency and may be grown in bigger forms. Undoped sodium iodide has a smaller decay constant compared to doped sodium iodide, which makes it attractive for fast imaging applications.

Table 3. Properties of Na and I

Element	Z	A (g/mol)	v	ρ (g/cm^3)	f	X_0 (cm)
Na	11	23.0	1	0.968	0.153	28.9
I	53	126.9	1	4.933	0.846	1.752

Density of NaI composite is calculated using the densities and mass fractions

$$\rho^{NaI} = 3.67 \ \ g/cm^3$$

For the radiation length of the NaI composite

$$X_0^{NaI} = 2.59 \ \text{cm}$$

and the the critical energy for the NaI crystal

$$E_c^{NaI} = 11.81 \ \text{MeV}$$

The Molière radius is computed and it has the following value

$$R_M^{NaI} = 16.9 \ \text{cm}$$

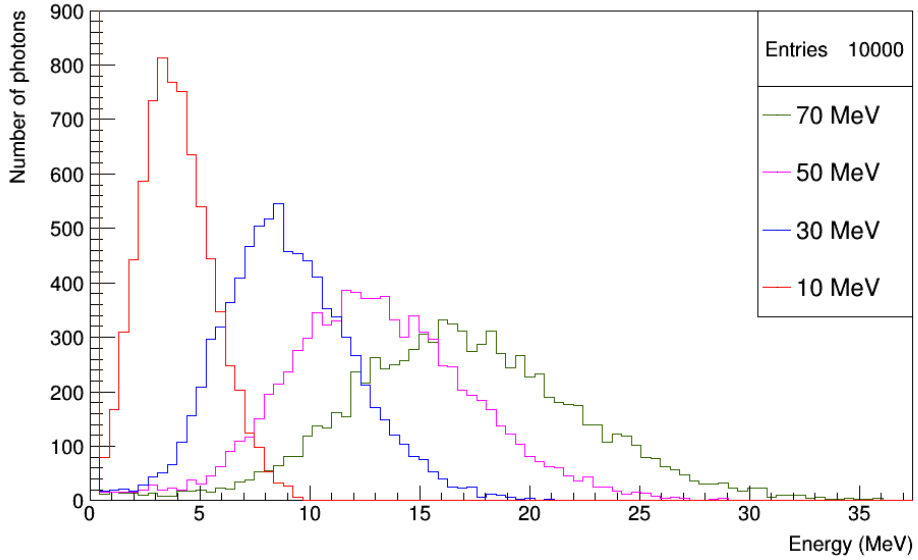

Figure 4. Various energy depositions in fiber of NaI scintillator.

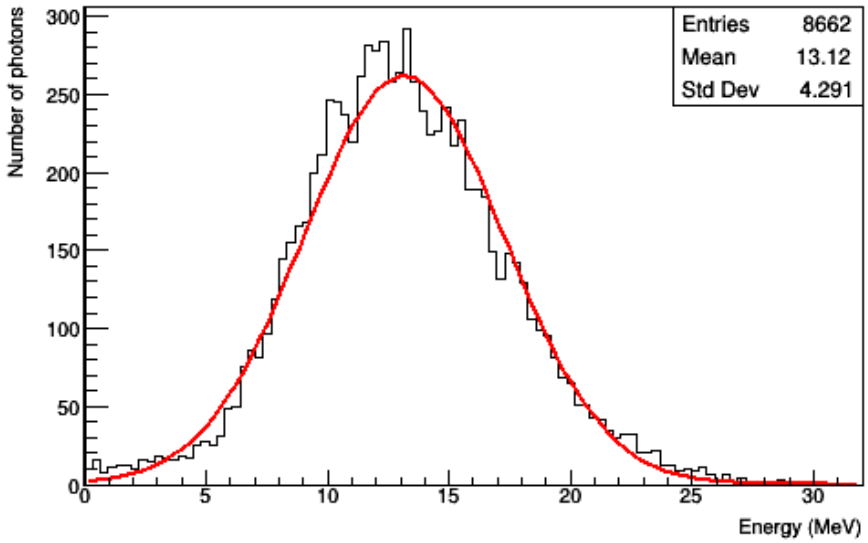

Figure 5. Energy deposition in fiber of NaI calorimeter for 50 MeV photons.

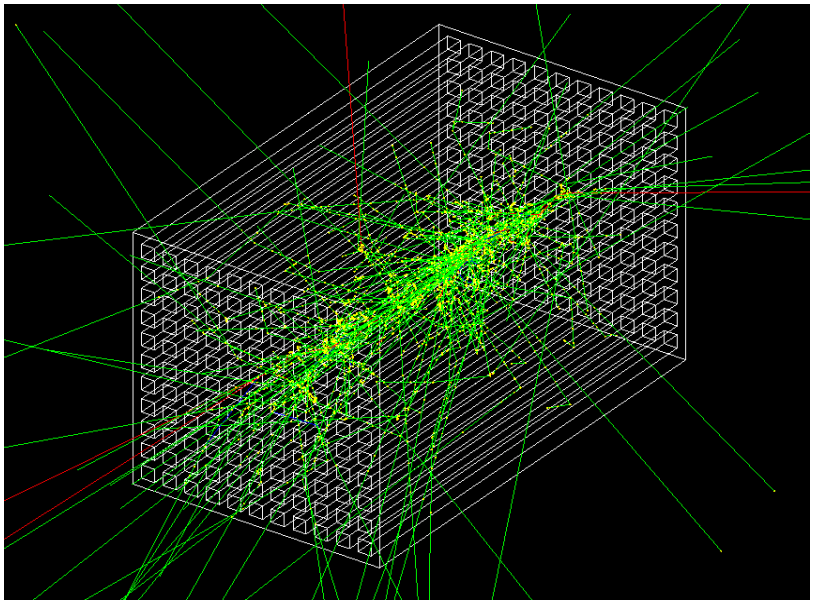

Figure 6. Simulation of electromagnetic shower in NaI 'spaghetti' calorimeter (initial 50 MeV photons).

5.3. Spaghetti (SpaCal) BGO calorimeter

Bismuth Germanate ($Bi_4Ge_3O_{12}$) is a high Z, high-density scintillation material. Due to the high atomic number of bismuth (83) and the material's high density, it is a very efficient gamma-ray absorber. Given the high Z value of the material, the photo fraction for gamma-ray absorption is high and as a result, very good peak-to-total ratios are observed. It is a relatively hard, rugged, non-hygroscopic crystal which does not cleave. The material does not show any significant self-absorption of the scintillation light. BGO scintillation crystals are used in applications where a high photofraction is required or because of its high detection efficiency.

Table 4. Component properties of the BGO scintillator

Element	Z	A (g/mol)	v	ρ (g/cm^3)	f	X_0 (cm)
Bi	83	208.98	4	9.78	0.671	0.636
Ge	32	72.64	3	5.32	0.175	2.359
O	8	15.99	12	1.43	0.154	24.083

Density of BGO composite is calculated using the densities and mass fractions

$$\rho^{BGO} = 7.13 \ \ g/cm^3$$

For the radiation length of the BGO composite

$$X_0^{BGO} = 1.11 \ \ cm$$

and the the critical energy for the BGO crystal

$$E_c^{BGO} = 8.22 \ \ MeV$$

The Molière radius is computed and it has the following value

$$R_M^{BGO} = 2.26 \ \ cm$$

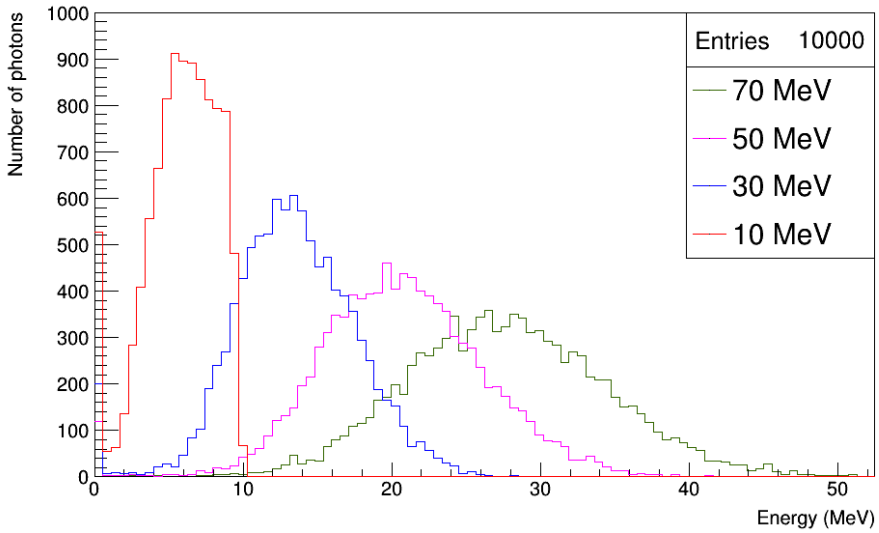

Figure 7. Various energy depositions in fiber of BGO scintillator.

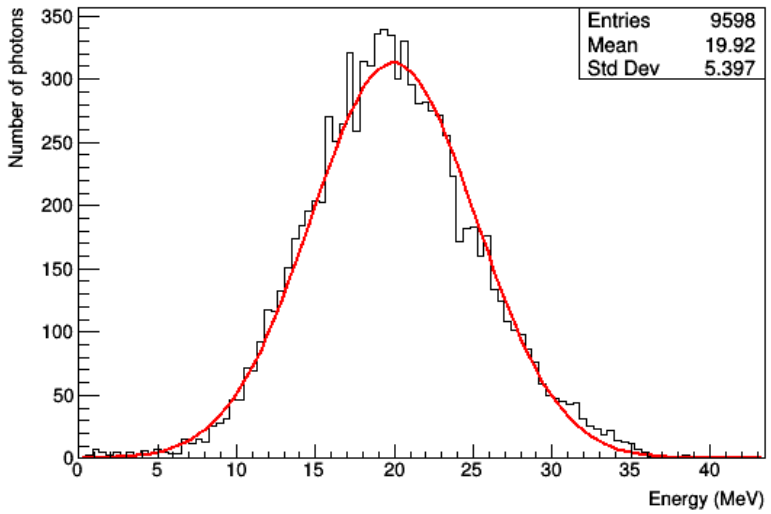

Figure 8. Energy deposition in fiber of BGO calorimeter for 50 MeV photons.

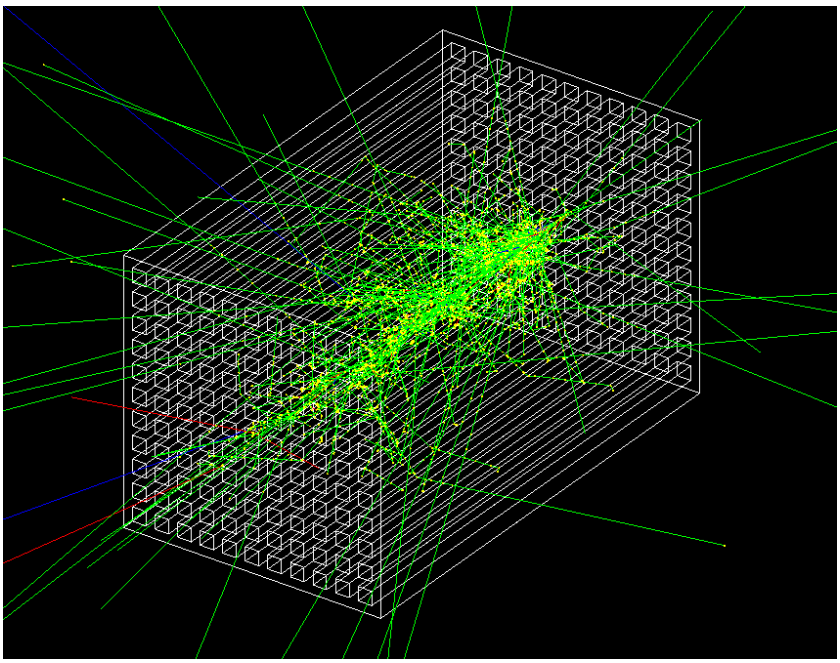

Figure 9. Simulation of electromagnetic shower in BGO ‘spaghetti’ calorimeter (initial 50 MeV photons).

5.4. Shashlik GaGG calorimeter

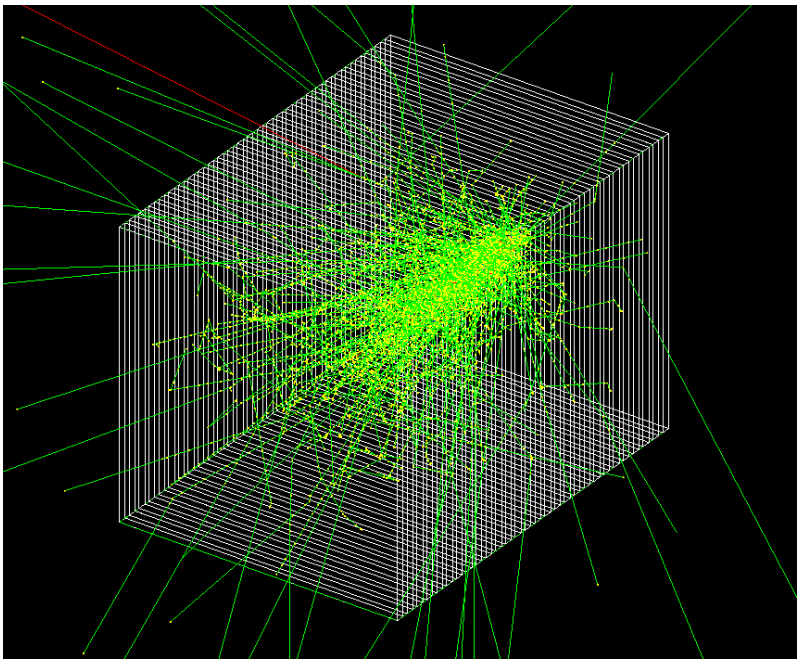

Figure 10. Simulation of electromagnetic shower in GaGG ‘shashlik’ calorimeter (initial 50 MeV photons).

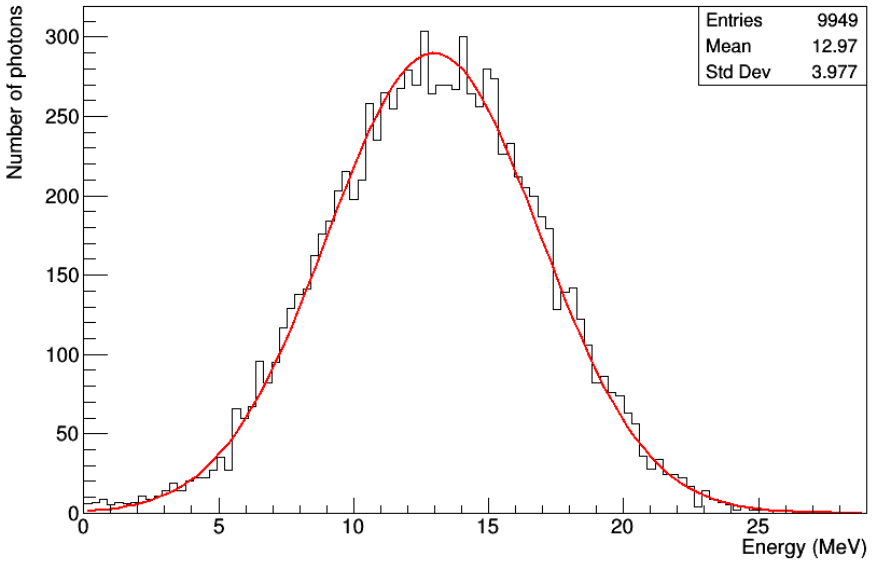

Figure 11. Energy deposition in layers of GaGG calorimeter for 50 MeV photons.

Energy resolution of fitted gaussian for E = 50 MeV is

$$\left(\frac{\sigma_E}{E}\right)_{GaGG} = 9.84\%$$

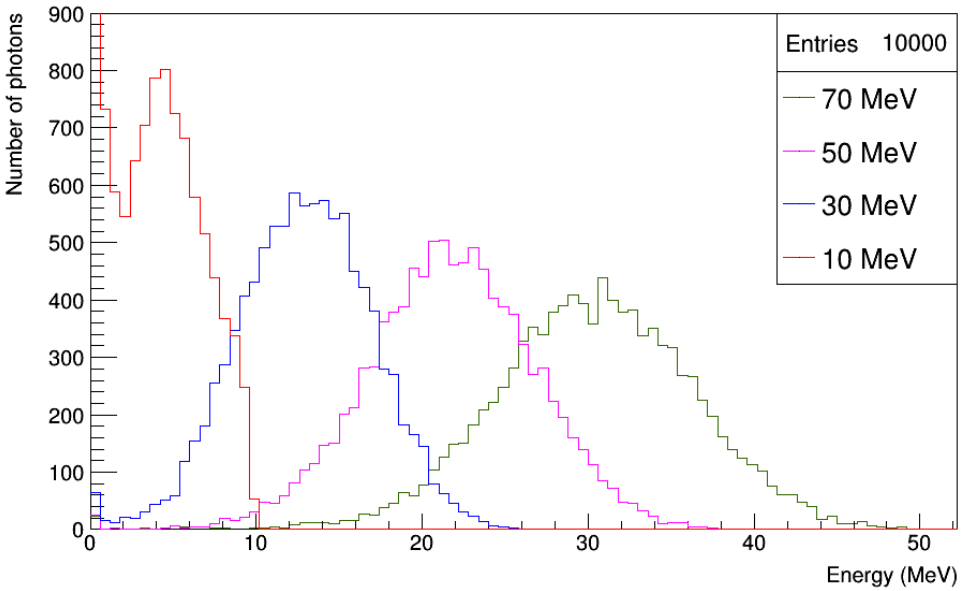

Figure 12. Various energy depositions in layers of GaGG scintillator.

5.5. Shashlik NaI calorimeter

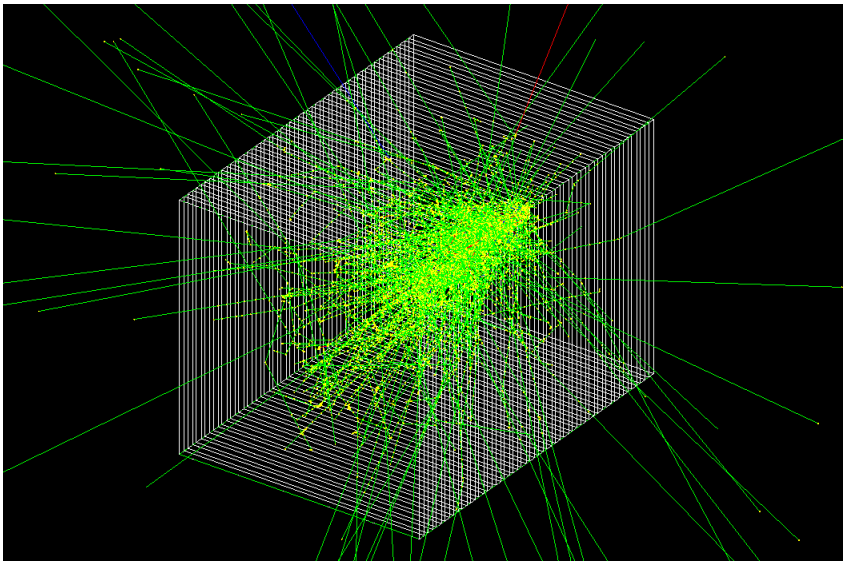

Figure 13. Simulation of electromagnetic shower in NaI 'shashlik' calorimeter (initial 50 MeV photons).

Energy resolution of fitted gaussian for E = 50 MeV is $\left(\frac{\sigma_E}{E}\right)_{NaI} = 8\%$

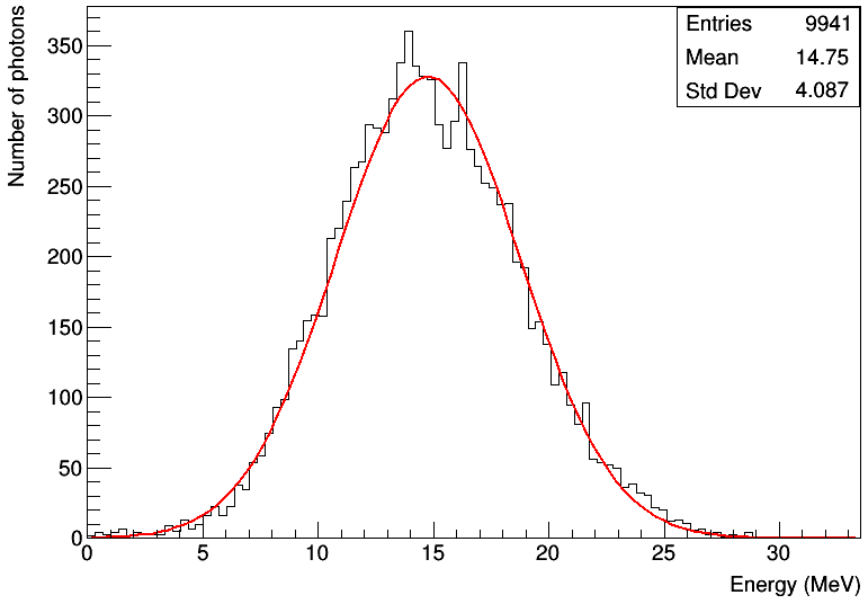

Figure 14. Energy deposition in layers of NaI calorimeter for 50 MeV photons.

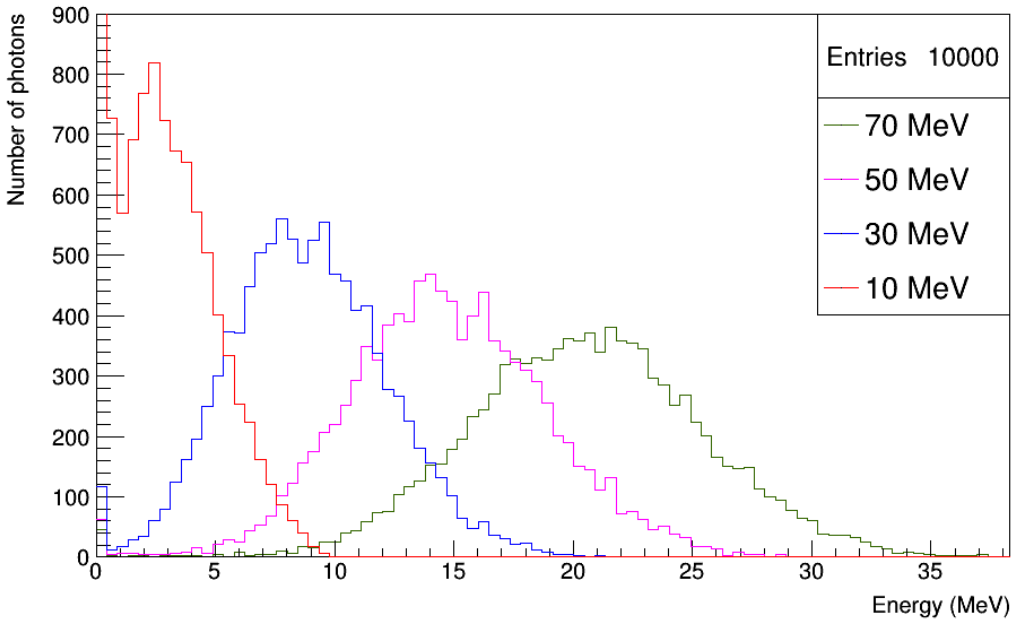

Figure 15. Various energy depositions in layers of NaI scintillator.

5.6. Shashlik BGO calorimeter

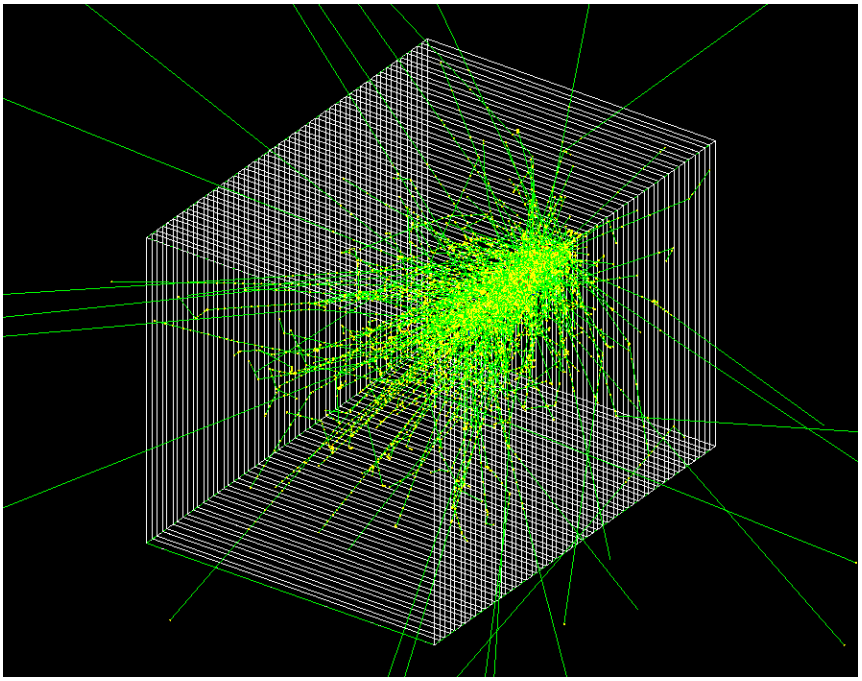

Figure 16. Simulation of electromagnetic shower in BGO 'shashlik' calorimeter (initial 50 MeV photons).

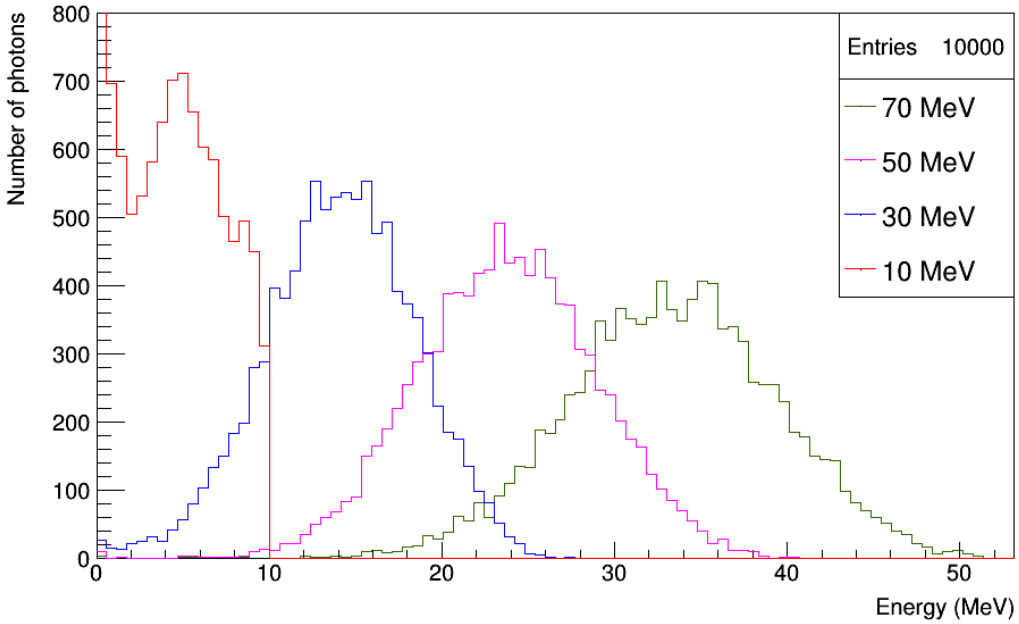

Figure 17. Various energy depositions in layers of BGO scintillator.

Energy resolution of fitted gaussian for E = 50 MeV is $\left(\frac{\sigma_E}{E}\right)_{NaI} = 10.29\%$

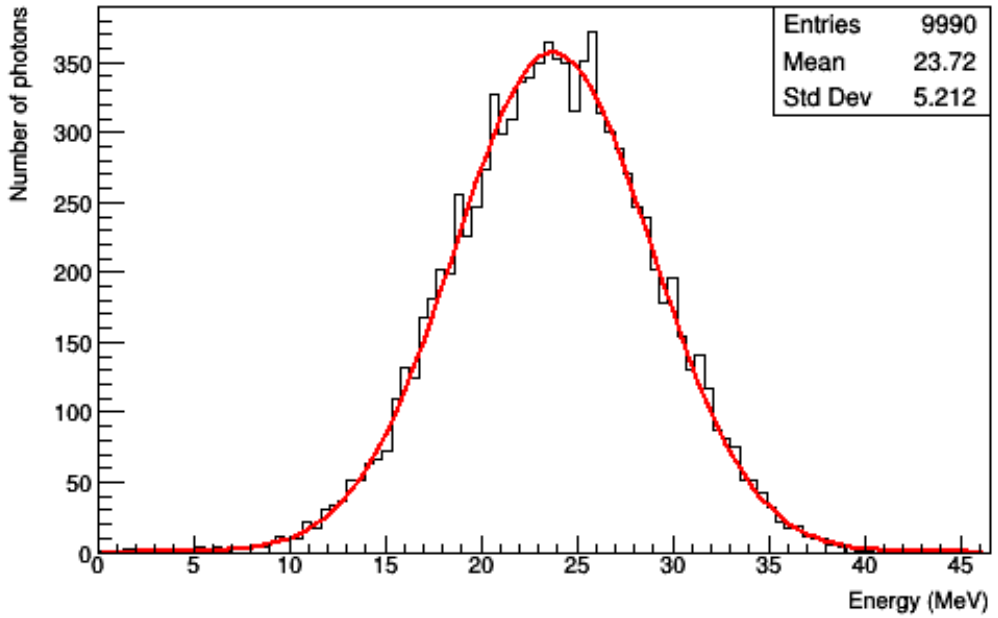

Figure 18. Energy deposition in layers of BGO calorimeter for 50 MeV photons.

6. Conclusion

In this study, three diffferent heterogeneous ‘spaghetti’ calorimetries and three alternate heterogeneous ‘shashlik’ calorimetries were simulated with the WCu absorber, using inorganic material compound: NaI, GaGG and BGO for each type. These procedure for investigating their resolution in recodring energy from the interaction of the radiation with the material in the calorimeters. The energy resolution was calculated for incident gamma particle energy from 10 to 1000 MeV for all of the heterogeneous calorimeters.

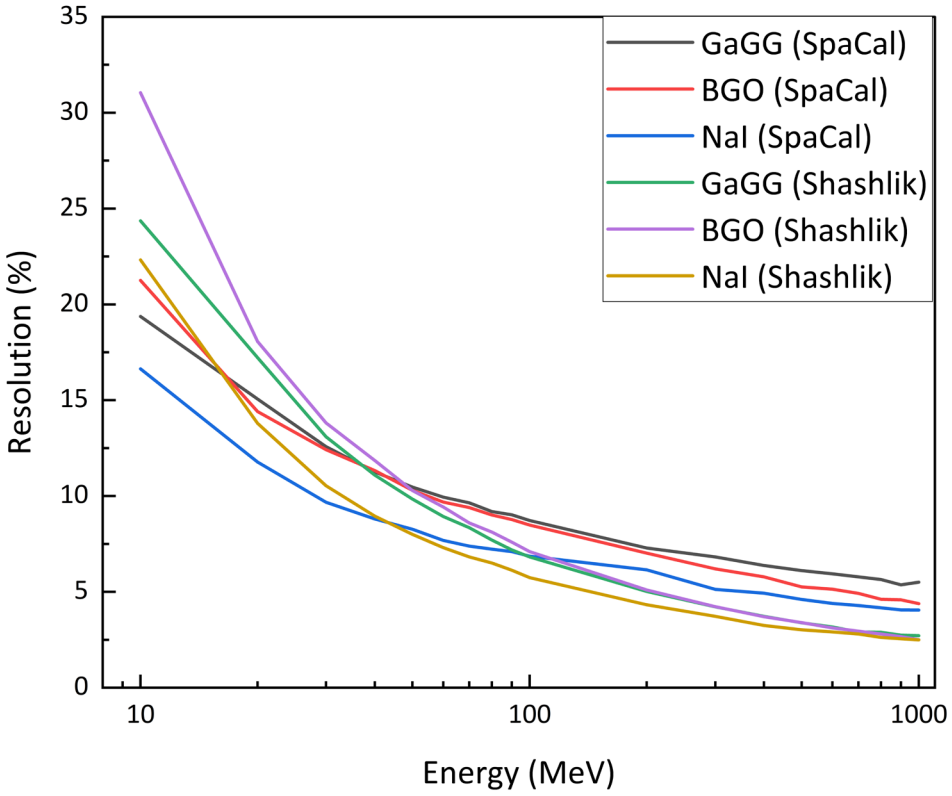

Figure 19. Comparison of different calorimeters.

For low energies, the ‘shashlik’ type calorimeter has a higher resolution, which gets smaller towards the higher energies as expected. And the resolution values do not differ greatly between the two types in the high-energy region. Specifically, the resolutions of the ‘shashlik’ types are lower with high energy radiation, for example, energy above 100 MeV. When come to the higher energy, the dispersion of the average deposition energy in the calorimeter becomes larger as seen in part 5. This leads to a decrease in the resolution with the fluctuations around the average value of each calorimeter.

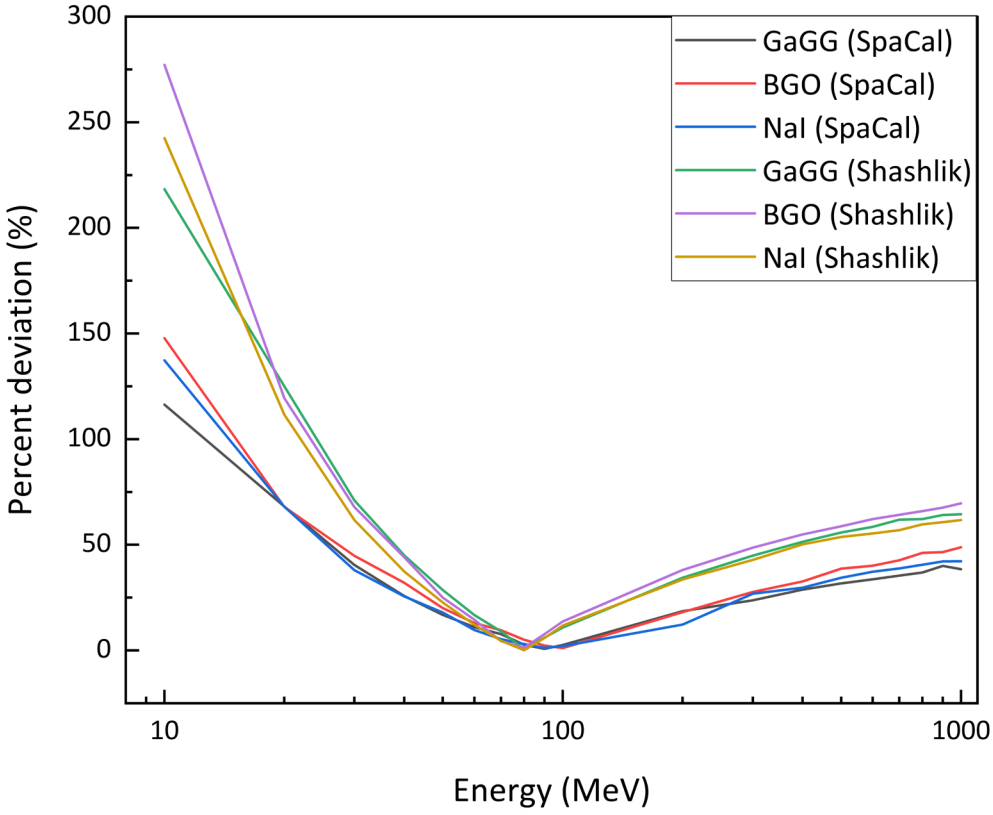

Figure 20. Comparison of percent deviation for different calorimeters.

The percent deviation values of the same calorimeter type are relatively similar, as seen in figure 20. However, in both the low and high energy zones, there is a definite difference between the two types. The results drop off quickly as approach high energy, and at around 90 to 100 MeV, the percentage deviation starts to rise once more.

Overall, GaGG material performs better resolution (7.24%) than other of SpaCal calorimeters for energy above 60 MeV, and that will be the BGO (5.1%) material for the Shashlik calorimeter type. NaI scintillator is the calorimeter material that has the lowest resolution for both types in either high or low energy. For energy below 60 MeV, BGO has a higher resolution than GaGG for both calorimeter types.

7. Reference

[1] E. Kokoulina, N. Barlykov, V. Dudin, A. Kutov, V. Nikitin, V. Riadovikov, R. Shulyakovsky, Study of soft photon yield in pp and AA interactions at JINR, The European Physical Journal Conferences 235:03003 (2020)

[2] C. Grupen, B. Shwartz. Particle Detectors, 2nd edition. Cambridge University Press, 2008.
[3] S. Masciocchi. Electromagnetic calorimeters (GSI and University of Heidelberg). Heidelberg, 28 June 2017.
[4] P, Jenni, P. Sonderegger. The high resolution spaghetti hadron calorimeter. CERN, Geneva, Switzerland 1987.
[5] P.V. Chliapnikov et al., Phys. Lett. B 141, 276 (1984).

8. Acknowledgments

I would like to express my sincere gratitude for my supervisor, prof Elena Kokoulina, for introducing me to calorimetry and GEANT4, as well as guiding me through the simulation of diffetent calorimeters and discussing the results with me.